Design and deployment of a physical channel simulator for performance analysis of free-space optical links

Davide Orsucci[a], Johannes Prell[a], Florian Moll[a],
Pia Lützen[a], Janis Surof[a], and Christian Fuchs[a]

[a]German Aerospace Center (DLR), Institute of Communications and Navigation, Münchener Straße 20, 82234 Weßling Germany

ABSTRACT

The use of free-space optical (FSO) links has the potential to significantly increase the data transmission rates compared to radio links and they enable the possibility of performing quantum communication. For the development of FSO components, including transmitters and receivers, and of novel communications protocols, it is essential to have the ability to comprehensively test the performance across several different communication scenarios – e.g., aircraft-to-ground, aircraft-to-aircraft, satellite-to-ground, and ground-to-satellite. To this end, we have built and deployed two fibre-based FSO channel simulators, having identical design, for testing optical communication in the C-band. These devices are capable of emulating in-the-lab the effects that the transmission through Earth's atmosphere would have on the received optical signal. Three parameters can be controlled and monitored in real-time: the average attenuation, the signal amplitude fluctuations and the signal phase fluctuations. The (constant) average attenuation emulates the end-to-end transmission loss, from signal source to sink, including the combined effect of geometric loss, due to long communication distances, of atmospheric absorption and fibre-coupling loss. The (time varying) amplitude fluctuations emulate the fast changes in signal intensity due to atmospheric turbulence and implementation specific disturbances like pointing errors. Finally, turbulence can also cause the phase of the signal to fluctuate in time and this effect can also be physically emulated. The amplitude and phase fluctuations time series can be loaded from previously measured data, or from synthetic data. These features allow testing the impact that the transmission through an FSO channel has on different communication schemes, including but not limited to telecommunication applications, like on-off keying and phase shift keying, and quantum communication applications, like quantum key distribution.

Keywords: Free-space optical communication, Channel simulator, Fading testbed, Scintillation, Amplitude fluctuations, Phase fluctuations

1. INTRODUCTION

In the rapidly evolving digital landscape, the demand for high-speed data transmission continues to grow. Satellites play a critical role in various applications, including Earth observations, internet connectivity to remote locations and scientific missions, all of which require efficient and reliable communication links. As these applications grow in complexity and data volume, traditional radio frequency (RF) links can become a significant bottleneck. RF links, while reliable, are often limited by bandwidth constraints, spectrum congestion, and susceptibility to interference, which can significantly hinder data transmission rates. Free-Space Optical (FSO) communication is a competitive alternative.[1]

Unlike RF links, FSO operates in a frequency range that is not subject to regulatory constraints or congestion, providing greater flexibility and availability. The much shorter wavelength, at the micrometer scale, enables data transmission bandwidths that are orders of magnitude higher than those of RF links.[2] Another unique feature of FSO is the capability to support quantum communication.[3] In fact, optical and near-infrared photons have energies in the electron-volt range, thus allowing individual quanta of light to be distinguished with single-photon detectors, a feat that is nearly impossible for RF photons. Additionally, as the diffraction-limited beam divergence is proportional to the wavelength, FSO systems can realize extremely collimated beams with terminals

Corresponding author e-mail: davide.orsucci@dlr.de

Environmental Effects on Light Propagation and Adaptive Systems VII, edited by Karin Stein, Szymon Gladysz, Proc. of SPIE Vol. 13194, 131940M
 · 0277-786X · doi: 10.1117/12.3033833

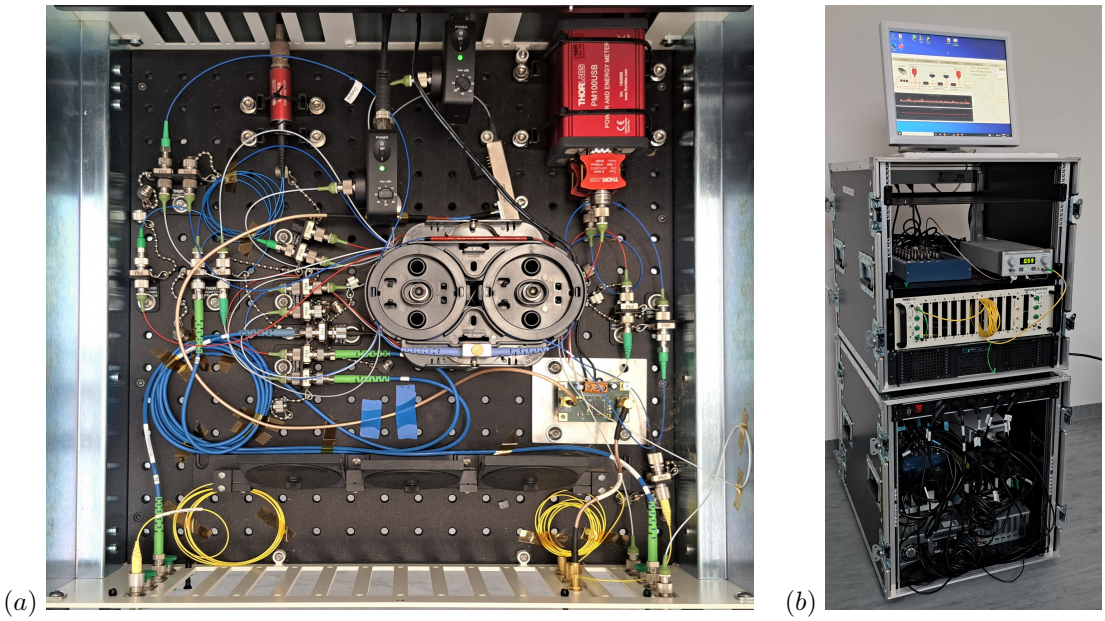

Figure 1. Channel simulator hardware. (*a*) Channel simulator optical setup mounted in a tray of a 19" rack. The input optical signal and the light from the calibration laser can enter from the ports visible on the bottom left (IN) and exit from the ports on the bottom right (OUT). (*b*) External appearance of the two channel simulators. Both setups are mounted in a 19" rack, stacked one on top of the other. Bottom rack: back view of the second specimen. Top rack: front view of the first specimen; a laser and a Data Acquisition (DAQ) are placed above the tray containing the optical setup, the control computer is placed underneath it. An external monitor and keyboard are connected to the first specimen for access to the control software.

of comparatively small sizes. The narrow beam divergence makes FSO inherently more secure, as it is much harder to intercept, eavesdrop, or spoof compared to RF communications. Finally, this smaller beam divergence and smaller terminals decrease the Size, Weight, and Power (SWaP) requirements, which is an important advantage for micro- and nano-satellites. This has led to the development of several high-performance Laser Communication Terminals (LCT), including the OSIRIS terminal developed in-house at the DLR Institute for Communications and Navigation.[4,5]

The main application of FSO is for link to Earth-orbiting satellites,[6] but larger communication distances can be supported, reaching the Moon[7] or even spacecraft in deep space.[8,9] Other FSO links configurations include ground-to-ground, aircraft-to-ground, aircraft-to-aircraft, each serving different potential use cases. These include establishing high data-rate links among nomadic and/or movable nodes[10] for resilience and reconfigurability in 5G/6G networks,[11] or enabling quantum communication through high-altitude platforms.[12] Each of these links features unique characteristics in terms of the observed optical power scintillation and phase fluctuations. For instance, for a fixed link geometry the observed scintillation index is typically stronger in an uplink channel than in downlink.[13,14] Further, for both classical and quantum communication phase coherence may be required. For instance, this is the case for classical communication based on phase-shift keying,[15] while in quantum communication and for QKD based on continuous variables[16] and for twin-field QKD protocols.[17] The physical channel simulators developed at DLR can serve for the development and testing of classical and quantum communication terminals, either requiring phase coherence or not.

2. CHANNEL SIMULATOR OVERVIEW

It is essential for the development and testing of FSO communication devices, either classical or quantum, to have the ability to perform integration tests in a quick and expedient manner. To this end, we have designed, built and deployed two *physical channel simulators*, a.k.a. *fading test-beds* or *channel emulators*. These are devices that are capable of emulating in-the-lab the effects that the transmission through atmosphere has on the received

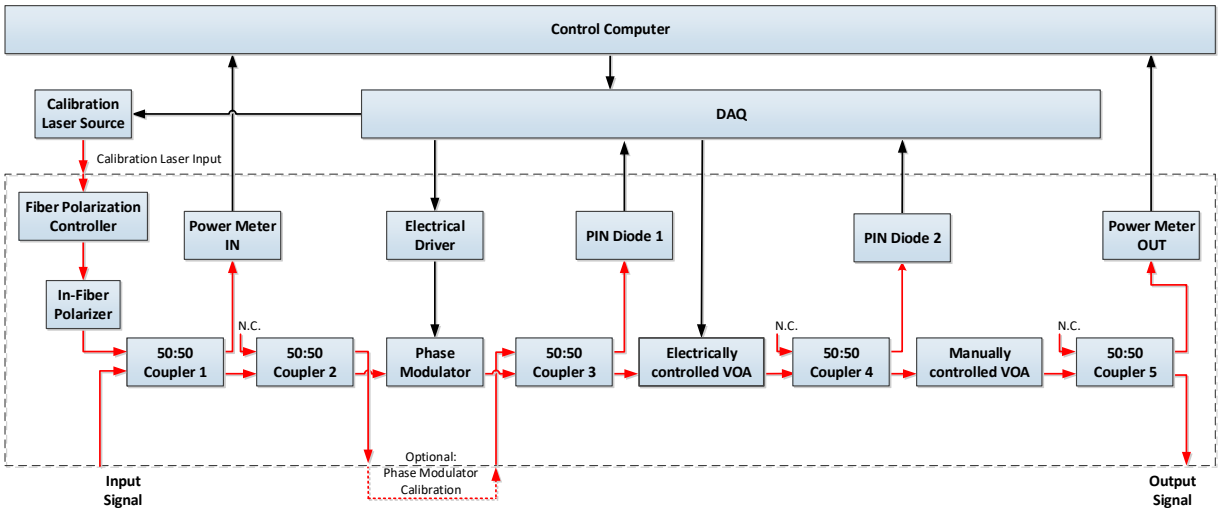

Figure 2. Functional block diagram of the channel simulator. The red arrows indicate optical connections, the black lines indicate electrical connections, while the dashed gray contour contains all the components mounted in the 19" tray. All communication to and from the control computer is via USB connections, all inputs and outputs of the Data Acquisition (DAQ) device are direct voltage controls and read-outs (except for the USB connection with the computer). The calibration laser source is connected via a single-mode fibre to a manual polarisation controller and then to an in-fibre polariser, after which all fibres in the setup are polarisation maintaining. The polarisation controller can be adjusted to minimise the losses at the in-fibre polariser. Three signal modulation devices are placed along the path of the optical signal: a phase modulator, an electrically controlled Variable Optical Attenuator (VOA) and a manually controlled VOA; an electrical driver is needed to amplify the current signal to the phase modulator. Four monitoring devices are also mounted in the setup: two Power Meters (PM) and two PIN Diodes (PD), used for calibration and monitoring of the optical modulation. Five 50:50 beam-splitters (couplers) are employed, with three having an input port which is Not Connected (N.C.).

laser signal. This allows the validation of the performance of a communication between co-designed transmitters and receivers under realistic channel conditions. This is typical in FSO communication development and several analogous devices have been built in the past.[18–20] A photo of the channel simulators we have built can found in Figure 1, while a block diagram of the electrical and optical components can be found in Figure 2.

The channel simulator has been designed so that three parameters can be independently controlled and set: the time-averaged signal attenuation, the fast signal amplitude fluctuations and the fast phase fluctuations. The signal attenuation control emulates the effect of power loss in the channel, averaged over time scales of seconds. The main contributions to the average channel loss are beam divergence and atmospheric absorption and they typically slowly change in time, due to changing link distance and varying atmospheric conditions. The amplitude fluctuation control emulates the fast changes in signal intensity due to effects such as beam wander and in-beam intensity scintillation, which are caused by the propagation through a turbulent atmosphere. This occurs at a much shorter time scale, usually in the order of milliseconds. Finally, phase fluctuation control can serve to emulate the time and spatial dependence of the phase of the signal at the receiver. In a real FSO channel this is also due to turbulence, causing a spatially-varying and time-varying atmospheric index of refraction which imprints a variable phase onto the transmitted signal.

In order to emulate an atmospheric channel the channel simulator has to work in a range between the maximum and the minimum signal intensity that is expected to be observed in the given scenario. For instance, consider a FSO link with fixed geometry where only optical power scintillation are relevant and suppose that a transmission time series of a 100-second period has to be emulated: the minimum and maximum then correspond to the maximum surge and minimum fade in intensity that is be observed in the time series. The channel simulator

normal transmission thus has to match the maximum signal intensity observed in the atmospheric channel time series, while the lower signal intensities are simulated by electronically increasing the attenuation as required.

Two essentially identical channel simulators have been built. The purpose of this redundancy is to support multiple projects at a time and to allow testing of communication scenarios requiring the establishment of two FSO links simultaneously, which is e.g. the case for entanglement distribution from a satellite.[21]

3. HIGH-LEVEL HARDWARE DESCRIPTION AND OPERATION PRINCIPLE

The channel simulator is based on a fibre-based setup mounted in a tray of a 19" rack. It employs polarisation-maintaining optical fibres which support the propagation of a single mode for wavelengths in the C-band with a fixed polarisation. Along the fibre are positioned optical and electro-optical components that allow us to manipulate a C-band optical laser signal propagating through the apparatus. Specifically, it is possible to electronically control the phase and the intensity of the signal, while a manually controlled attenuator can be used to set the mean attenuation.

The channel simulator is also equipped with two Power Meters (PM) and two PIN Diodes (PD) to read out the signal at different points of the optical path. The PDs are read out synchronously with the settings of the attenuations, which allows to verify whether the channel simulator operation is nominal. Furthermore, these measurement devices allow to perform on-demand an automated recalibration of the setup whenever required. The main reason for having these four measurement devices is to obtain a characterisation of the response curves of the phase modulator and of the electronic VOA. Specifically, the PMs provide a slow but calibrated readout of the optical signal, directly converting the readout voltage to a power. On the other hand, the PDs provide a fast response which can be used to track the fluctuating signal with millisecond time resolution. The calibration curves are therefore obtained by correlating the readout voltages of the PD with the power observed by the PMs. Finally, the total attenuation can also be measured via the PMs, since one (PM IN) is located right after the optical input and the other (PM OUT) right before the optical output.

The setup presents in total five 50:50 beam-splitters along the main path connecting the optical input and output of the channel simulator: four beam-splitters are used to couple the signal to the two PM and the two PD, while one more beam-splitter is needed to create an input port to a Mach-Zehnder interferometer having the electro-optical phase modulator placed in one of its arms. In normal operation mode, the second external arm of the Mach-Zehnder interferometer is disconnected, and it has to be connected only for calibration of the phase modulator. Each 50:50 beam-splitter introduces around 3 dB of attenuation to the signal, totalling 15 dB of attenuation. If the second arm of the interferometer is connected, the attenuation depends on the phase difference of the two arms and fluctuates randomly on a sub-second time scale. The insertion losses of the phase modulator and of the VOA are a couple of dB, resulting in a total transmission loss that significantly exceeds 15 dB. Higher attenuation can be obtained by setting the electronic and manual Variable Optical Attenuator (VOA) to non-zero values, which can introduce up to 25 dB and 50 dB of attenuation, respectively.

A laser source with an emission wavelength of 1550 nm is also included in the setup. Its optical signal can be fed into the apparatus to be used as a reference signal for the calibration procedures and, possibly, to emulate the presence of background light while operating the device together with FSO communication terminals. The laser light is naturally stable in polarisation, but its output is in a single-mode fibre, rather than in a polarisation maintaining fibre. The mating sleeve from single-mode to polarisation maintaining fibre can then result in partial signal loss due to polarisation mismatch. It is possible to modify the polarisation state of the light prior to the injection into the polarisation maintaining fibre via a manual polarisation controller at the input, allowing for optimisation of the coupling with the polarisation-maintaining fibre. The use of polarisation maintaining fibres is a design choice that entails a non-trivial trade-off in capabilities. On the one hand, it precludes the complete testing of optical communication transceivers that modulate of the state of polarisation, including e.g. polarisation-based QKD protocols. On the other hand, it has the advantage of being more stable, allowing the direct calibration of the applied phase modulation by observing the intensity modulation it causes at an output port of a Mach-Zehnder interferometer.

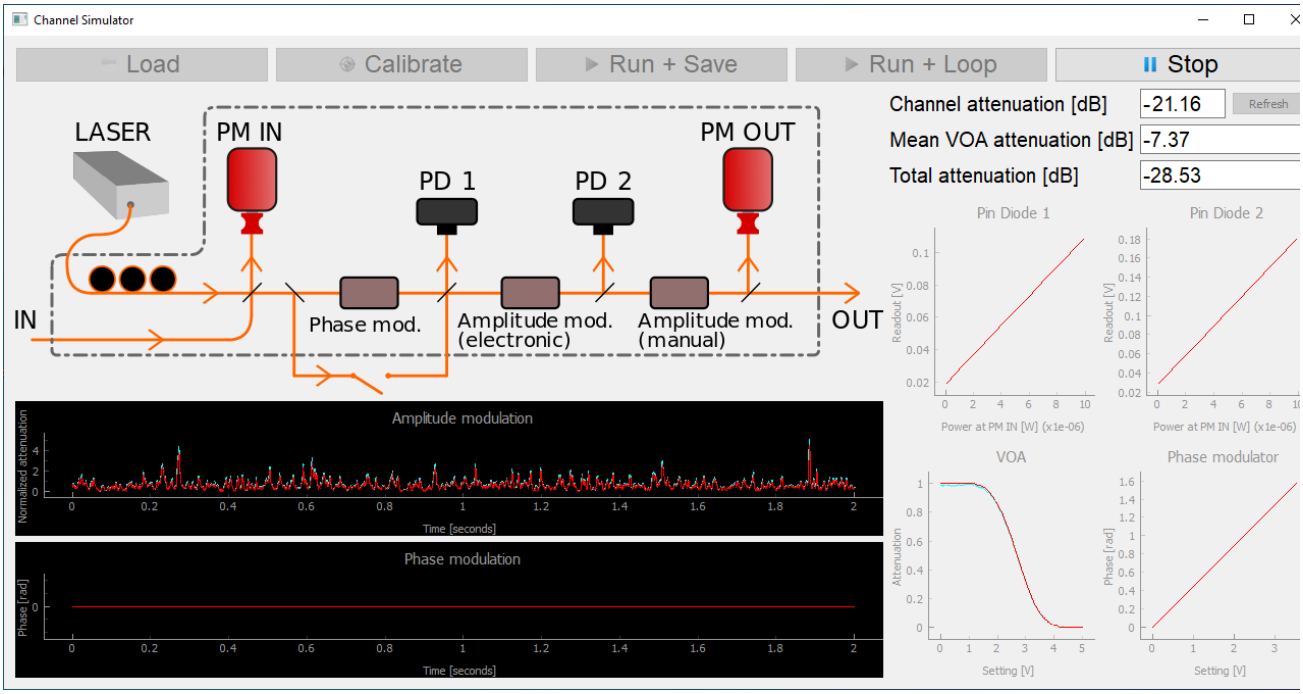

Figure 3. Appearance of the channel simulator GUI while running. Top left: illustrative block diagram of the optical part of the channel simulator setup; the components within the dashed line are mounted in the tray; each of the diagonal lines along the path from IN to OUT represents a 50:50 beam-splitter. Bottom left: power scintillation time series, set values (in red) and re-read values (in cyan). The phase modulation requires an interferometer to be read out and is not shown. Top right: current channel attenuation and the mean VOA attenuation that needs to be added in order to emulate the currently selected scintillation time series. Bottom right: calibration curves. The voltage of the PIN diodes is correlated to the power recorder by the PM IN, the phase modulator calibration is assumed to be linear and take from the data-sheet, while for the VOA both the bare calibration data (in cyan) and its isotonic regularisation (in red) are shown.

4. CONTROL AND READOUT SOFTWARE

Custom software has been developed to manage electronic inputs and outputs for the channel simulator electro-optical components, enabling the loading and reproduction of phase and amplitude fluctuation time series within the hardware. The time series can originate from experimental data or be the result of simulations. The control software runs on a blade computer embedded within the rack, featuring a simple Graphical User Interface (GUI) that facilitates user interaction. However, all the underlying Python control code is fully accessible, allowing for customization when needed. The software employs multi-threading, which enables simultaneous functioning of the GUI front-end and the control and readout back-end.

The electro-optical components are voltage-controlled, with electronic inputs provided via a Data Acquisition (DAQ) device connected to the control computer through a USB interface. The DAQ also manages the laser intensity during calibration and reads the PD measurement values. The PMs are directly connected to the control computer via USB and provide calibrated power measurements in SI units (Watts). These power meters are rather slow, refreshing at only a few Hz, e.g. due to communication lag inherent in the USB protocol. On the other hand, the PDs offer fast response times and are used to monitor emulated amplitude and phase fluctuations in real time. However, their output voltage is uncalibrated, since the readout value depends also on the employed electronic gain, and can exhibit non-linear dependence when close to the saturation thresholds. By comparing the PD readouts with the calibrated PM values, this power-voltage relationship can be assessed and calibrated. Once the PDs have been calibrated, these can in turn be employed to calibrate the response curve of the VOA, as well as the total transmission of the channel simulator.

The response curve of the VOA, giving the observed attenuation as a function of the input voltage, has to be characterised and inverted in order to obtain required control curve, i.e. giving the required input voltage to obtain the desired attenuation. The optical transmission decreases for increasing voltages, but the dependence is very weak at low voltages, i.e., the derivative of the curve is very flat, with derivative very close to zero. When inverting the function this would result in a control function that has a very large derivative in the input voltage, resulting in an ill-conditioned control. To avoid this we thus restrict the operation of the VOA to 95% of its maximum transmission. Furthermore, note that the scintillation of an FSO channel results not only in fading but also in surges, i.e., the instantaneous received power can exceed the average received power $\langle P \rangle$. The VOA is only capable of introducing transmission losses (it cannot amplify the input power) and therefore it needs to be operated in a regime where the maximum emulated channel surge $P_{\max}$ corresponds to 95% of its maximum transmission. As a result, to be able to emulate the scintillation, the VOA introduces further losses in the channel simulator compared to the case in which the VOA input is set to 0 V. This extra loss depends on the strength of the scintillation in the emulated time series and is equal to $10 \log_{10}(0.95 \cdot \langle P \rangle / P_{\max})$ dB.

5. CALIBRATION PROCEDURE

The calibration process consists of three main steps that we will now describe.

In the first calibration phase, the laser power is gradually and slowly increased while maintaining the VOA input voltage at 0 V to prevent any additional attenuation. During this process, the readings from all PMs and PDs are recorded simultaneously. This step enables the calibration of the PD response curves against the calibrated responses of the PMs. The laser source requires several seconds to settle into a new stable configuration after the setting of its voltage bias and the linearity of its power output in the voltage bias is not guaranteed, hence the need to infer its power via the PMs rather than from the laser bias voltage.

In the second calibration phase, the laser intensity is set to a fixed value, waiting a few seconds so that it settles in a stable configuration, and the transmission of the electronically controlled VOA is varied. We leverage the fact that the PDs have been just calibrated to use them to measure the transmission of the VOA as a function of the applied voltage. The fast response time of PDs allows to perform the measurement very rapidly compared to the typical relaxation times of the laser source. However, due to noise in power measurements at different voltages, the VOA calibration curve may be non-monotonic, making it impossible to directly invert it to obtain a control curve. To address this problem, an L_1 isotonic regression algorithm is applied to regularize the data and produce the closest monotonic calibration curve.[22] Specifically, given the measured data points $\{y_i\}_i$, where the index i represents equally spaced input voltages, a new set of values $\{\hat{y}_i\}_i$ is generated, satisfying $\hat{y}_i \geq \hat{y}_j$ for each $i < j$ (i.e., are monotonically non-increasing), while minimizing the L_1 distance given by $\sum_i |\hat{y}_i - y_i|$.

In the third and last part of the calibration, the VOA is again set to 0 V and the PMs are used to precisely measure the laser power at the input and at output by taking the average of several measurements. This procedure assumes that the beam-splitters are approximately balanced and that they have negligible insertion losses, meaning that the power values received by the PM IN and PM OUT are given by $P_{\text{PM IN}} \approx \frac{1}{2} P_{\text{in}}$ and $P_{\text{PM OUT}} \approx P_{\text{out}}$, where P_{in} is the power injected in the input port and P_{out} is the power exiting at the output port. The total transmission η of the channel simulator can then be approximated as $\eta \equiv P_{\text{out}}/P_{\text{in}} \approx P_{\text{PM OUT}}/(2P_{\text{PM IN}})$. Note that the values $P_{\text{PM OUT}}$ and $P_{\text{PM IN}}$ are read from two different PM, which may have slight differences in their calibrations. Therefore, in case a more accurate measurement of the channel loss is required, we recommend directly measuring the power at the input and output of the channel simulator using a single calibrated external PM to eliminate the reliance on the aforementioned assumptions.

We remark that there is no on-line calibration procedure for the phase modulator, as doing so would require to set-up an interferometric measurement and use trigonometric functions to fit the observed interference pattern. Furthermore, from an off-line characterisation of the device it was found that the component has an excellent linearity of the phase setting in the applied voltage. We have thus opted for directly using the quarter wavelength value $V_{\pi/2} = 3.5\,\text{V}$ provided in the datasheet.

The results of the calibration procedure are converted into piecewise linear functions that are displayed in corresponding plots inside the user interface main window. The inverses of the VOA response function and of the (fixed) phase modulator response function can then be used to compute which voltage setting has to be applied in order to obtain the desired amplitude and phase modulation.

6. SUMMARY AND CONCLUSIONS

In this paper, we have presented of a physical channel simulator for FSO communication systems. The developed setup utilises polarisation-maintaining optical fibres and a series of optical and electro-optical components to accurately emulate the effects of the atmospheric turbulence on FSO links. This includes independent control of signal attenuation, amplitude fluctuations and phase fluctuations, all of which are essential for emulating FSO communication channels. The channel simulator incorporates both fast and slow power measurement devices: two power meters provide calibrated slow measurements and a measurement of the total channel attenuation, while two PIN diodes offer fast readouts, enabling the on-line monitoring of the emulated channel.

A custom multi-threaded control software has been developed to manage the electronic inputs and outputs. This allows the user to load scintillation time series from experimental data or simulations and reproduce them in real time. The software also supports calibration procedures including, for instance, an automated process to measure the response curve of the electronically controlled VOA.

The physical channel simulators have already been employed for testing and developing FSO communication systems, for both classical and quantum communication applications. Through the implementation of two identical simulators, these devices will be able to support multiple projects or more complex communication scenarios involving two simultaneous FSO links. This is required in some quantum communication scenarios, including entanglement distribution and measurement-device-independent QKD protocols.

ACKNOWLEDGMENTS

The work was supported by the project QuNET funded by the German Federal Ministry of Education and Research (BMBF).

REFERENCES

[1] Khalighi, M. A. and Uysal, M., "Survey on free space optical communication: A communication theory perspective," *IEEE communications surveys & tutorials* **16**(4), 2231–2258 (2014).

[2] Poliak, J., Calvo, R. M., and Rein, F., "Demonstration of 1.72 Tbit/s optical data transmission under worst-case turbulence conditions for ground-to-geostationary satellite communications," *IEEE Communications Letters* **22**(9), 1818–1821 (2018).

[3] Orsucci, D., Kleinpaß, P., Meister, J., De Marco, I., Häusler, S., Strang, T., Walenta, N., and Moll, F., "Assessment of practical satellite quantum key distribution architectures for current and near-future missions," *arXiv preprint arXiv:2404.05668* (2024).

[4] Schmidt, C., Brechtelsbauer, M., Rein, F., and Fuchs, C., "Osiris payload for DLR's BiROS satellite," in [*International Conference on Space Optical Systems and Applications 2014*], (2014).

[5] Fuchs, C., Moll, F., Poliak, J., Reeves, A., and Schmidt, C., "Optical satellite links at DLR," in [*Free-Space Laser Communications XXXV*], **12413**, 34–41, SPIE (2023).

[6] Hemmati, H., "Near-earth laser communications," in [*Near-Earth Laser Communications, Second Edition*], 1–40, CRC press (2020).

[7] Nonay, J. R., Fuchs, C., Orsucci, D., Schmidt, C., and Giggenbach, D., "SelenIRIS: a Moon-Earth optical communication terminal for CubeSats," in [*2022 IEEE International Conference on Space Optical Systems and Applications (ICSOS)*], 186–195, IEEE (2022).

[8] Hemmati, H., Biswas, A., and Djordjevic, I. B., "Deep-space optical communications: Future perspectives and applications," *Proceedings of the IEEE* **99**(11), 2020–2039 (2011).

[9] Biswas, A., Srinivasan, M., Andrews, K., Alerstam, E., Velasco, A., Wright, M., Kovalik, J., Douglas, B., Allmaras, J., Van Rhein, V., et al., "Deep space optical communications technology demonstration," in [*Free-Space Laser Communications XXXVI*], **12877**, 32–43, SPIE (2024).

[10] Shrestha, A. and Brechtelsbauer, M., "Transportable optical ground station for high-speed free-space laser communication," in [*Laser Communication and Propagation through the Atmosphere and Oceans*], **8517**, 44–52, SPIE (2012).

[11] Calvo, R. M., de Cola, T., Poliak, J., Macrì, L., Papa, A., Ayvasik, S., Babaians, E., and Kellerer, W., "Optical feeder links for future very high-throughput satellite systems in b5G networks," in [*2020 European Conference on Optical Communications (ECOC)*], 1–4, IEEE (2020).

[12] Giggenbach, D., Horwath, J., and Epple, B., "Optical satellite downlinks to optical ground stations and high-altitude platforms," in [*2007 16th IST Mobile and Wireless Communications Summit*], 1–4, IEEE (2007).

[13] Giggenbach, D., Parthasarathy, S., Shrestha, A., Moll, F., and Mata-Calvo, R., "Power vector generation tool for free-space optical links—PVGeT," in [*2017 IEEE International Conference on Space Optical Systems and Applications (ICSOS)*], 160–165, IEEE (2017).

[14] Carrillo-Flores, A., Giggenbach, D., Shrestha, A., and Knopp, M. T., "Absolute power vectors for the optical LEO uplink channel," in [*COAT2023*], (2023).

[15] Salz, J., "Coherent lightwave communications," *AT&T technical journal* **64**(10), 2153–2209 (1985).

[16] Laudenbach, F., Pacher, C., Fung, C.-H. F., Poppe, A., Peev, M., Schrenk, B., Hentschel, M., Walther, P., and Hübel, H., "Continuous-variable quantum key distribution with gaussian modulation—the theory of practical implementations," *Advanced Quantum Technologies* **1**(1), 1800011 (2018).

[17] Lucamarini, M., Yuan, Z. L., Dynes, J. F., and Shields, A. J., "Overcoming the rate–distance limit of quantum key distribution without quantum repeaters," *Nature* **557**(7705), 400–403 (2018).

[18] Shrestha, A., Giggenbach, D., Mustafa, A., Pacheco-Labrador, J., Ramirez, J., and Rein, F., "Fading testbed for free-space optical communications," in [*Advanced Free-Space Optical Communication Techniques and Applications II*], **9991**, 16–25, SPIE (2016).

[19] Geisler, D., Wong, K., Schulein, R., Wang, J., Bedrosian, P., Hakimi, F., Schieler, C., Spellmeyer, N., Caplan, D., Robinson, B., et al., "Atmospheric emulation and testing methodology for laboratory verification of FSO communications transceivers," in [*2019 IEEE International Conference on Space Optical Systems and Applications (ICSOS)*], 1–5, IEEE (2019).

[20] Ivanov, H., Marzano, F., Leitgeb, E., and Bekhrad, P., "Testbed emulator of satellite-to-ground fso downlink affected by atmospheric seeing including scintillations and clouds," *Electronics* **11**(7), 1102 (2022).

[21] Lu, C.-Y., Cao, Y., Peng, C.-Z., and Pan, J.-W., "Micius quantum experiments in space," *Reviews of Modern Physics* **94**(3), 035001 (2022).

[22] Rote, G., "Isotonic regression by dynamic programming," in [*2nd Symposium on Simplicity in Algorithms (SOSA 2019)*], Schloss Dagstuhl–Leibniz-Zentrum für Informatik (2019).